Advances in Science and Technology Research Journal

Advances in Science and Technology Research Journal, 2025, 19(8), 205–216
https://doi.org/10.12913/22998624/205033
ISSN 2299-8624, License CC-BY 4.0

Received: 2025.03.22
Accepted: 2025.06.15
Published: 2025.07.01

Experimental studies on optimal actuator shape in active vibration control of triangular plates

Romuald Kuras[1*], Andrzej Kawalec[2], Sebastian Hajder[1], Adam Brański[1]

[1] Department of Electrical and Computer Engineering Fundamentals, Rzeszów University of Technology, ul. Wincentego Pola 2, Rzeszów, 35-959, Poland
[2] Department of Manufacturing Techniques and Automation, Rzeszow University of Technology, ul. Wincentego Pola 2, Rzeszów, 35-959, Poland
* Corresponding author's e-mail: r.kuras@prz.edu.pl

ABSTRACT

Piezoelectric actuator, as one of the components of active vibration control system, influences the effectiveness of vibration reduction. To make the reduction process most effective, the efficiency of all its components must be maximised. Hence, optimising the shape of piezoelectric actuators (PZT) in terms of efficiency contributes to increasing the efficiency of vibration reduction process. The paper presents an experimental verification of a new approach to optimising the shape of PZT. The objective function was to minimise structure vibrations. The result of optimisation process was a PZT shape that most effectively reduces plate vibration. The paper compares the regular PZT shapes with the PZT giving the best efficiency. A simply supported triangular plate was chosen as the research object. An active vibration reduction system using closed-loop control was built to verify the model. The control system was implemented on ESP-32 development board, loudspeaker was used to induce vibrations in the plate. The validity of the optimised PZT shape in active vibration reduction of triangular plates was confirmed by the closed-loop control time courses.

Keywords: triangular plate, piezoelectric actuator, active vibration reduction, active vibration control, closed-loop control.

INTRODUCTION

Active vibration control is applied to various structural elements, including beams, shells, plates, shafts and trusses. To improve the efficiency of this process, different types of controllers can be investigated the actuator used also plays a significant role. Piezoelectric actuators (PZT) are commonly used in active vibration control. The effectiveness of vibration reduction process is influenced by geometric parameters and location of the actuator on the structure.

PZT consists of two electrodes with a layer of piezoelectric material between them. The optimisation of PZT geometrical parameters can be divided into two approaches. The first approach that optimises the PZT geometry deals with optimisation of the electrode material distribution [1, 2], while the second approach deals with optimisation of the piezoelectric material distribution (or the whole actuator) [3, 4]. Aridogan and Basdogan [5] provide a thorough review of the problem of active vibration and noise control in two-dimensional structures using piezoelectric elements. The articles classifies controllers and evaluates their performance in reducing vibration of plates with varying boundary conditions. Another review paper dealing with piezoelectrics as such is that published by Al-Obiedy and Al-Helli [6], which presented a collection of research in the field of enhanced piezoelectric properties. Liu and Xiao [7] determined the optimum shape of PZT for two-dimensional structures. In this work, the researchers identified the areas covered with the piezoelectric material in a laminated rectangular cantilever plate. The resulting areas of the piezoelectric material coverage were replaced by regular shapes in the form of a finite number of square PZT patches.

The problem of the placement of actuators and their shape is important from the point of view of reducing vibrations of a given mode shape. In [8], a thin rectangular plate was studied in the context of active vibration control, using a disc-shaped actuator. Its position resulted in a zero effect for the second mode shape. Different shapes of PZT actuators were investigated to determine their effect on a sensor-actuator hybrid in [9]. The examined actuators were square or disc-shaped with a hole cut out for the sensor part.

This paper is an experimental work (first of all), so important issues are those related to the experiment itself. The implementation of simply supported boundary condition for the plate was similar to [9], except that in addition to the V-groove, a chamfer was also made on the plate – so that the entire edge of the plate lay on one line in the V-groove. Another difference is that heat-shrinkable sleeves were used around the edge of the plate instead of universal sealant. A plate with a simply supported boundary condition was also tested in [11], where two opposite boundaries were simply supported. A comprehensive work covering both theory and experiment is [12], in which a simply supported plate was investigated and the optimal placement of actuators was determined; rectangular actuators were used. The plate was supported on the frame to mimic the simply supported boundary condition. Rahman and Darus [13] proposed the AVC-P controller, which had the ability to reduce vibrations of flexible structures. The controller was a classical proportional-gain controller. In this paper, a PID controller was also used, but the integral tuning parameter was kept at a relatively low level and not completely eliminated.

The optimisation of the actuator shape can be performed under different optimisation criteria. For example, the objective function can be the minimisation of the control energy required to reach the desired state [14]. The objective function can also be derived from the theory of mechanical vibrations and the PZT-plate interaction. Before solving the problem of determining the optimal shape of PZT for 2D structures, it was necessary to start from the one-dimensional case, which was presented in [15, 16]. The objective function was to minimise a mathematical expression that depends on the bonded place of the PZT and the length of fibres that PZT consist of. For the plate, this means first finding a common point for all PZT fibres and then optimising the arm lengths of each force pair [17]. In this way the contour of an a-PZT was obtained. Using the derived formulae for the beam and analogous ones for the plate, it has been shown that the common point for all PZT fibres should be the point where the bending moment of the plate reaches its absolute extreme. This is due to the fact that an effect of PZT is proportional to the value of the plate bending moment at this point. Hence, if one needs this effect to reach its maximum value, the bending moment should be maximised. A simply supported triangular plate has only one such point and this point was designated as the common point of all PZT fibres.

The aim of the article was to experimentally verify the research presented in [17]. In the cited article, optimal shape of the PZT (a-PZT) was obtained for triangular plate. This shape ensured maximum efficiency for the steady state. A natural consequence of the research carried out was to perform an experiment that would confirm or refute the obtained conclusions. This paper compared regular PZT shapes (circular c-PZT, square s-PZT) with a-PZT in active vibration reduction of triangular plates. To achieve this aim, a test rig was set up with a PI controller implemented on ESP32 development board. The controller tuning parameters were selected experimentally and three identical simply supported triangular plates with actuators glued to them were tested. The results were compared with those obtained by steady-state analytical and numerical calculations.

MODEL OF THE PLATE

The governing equation of transverse vibration of triangular plate is based on Kirchhoff-Love theory for thin plates [18],

$$D\nabla^4 w(x,y,t) + \rho h_p \frac{\partial^2 w(x,y,t)}{\partial t^2} = f(x,y,t) \quad (1)$$

In the steady state the equation takes the form,

$$\nabla^4 w(x,y) - \frac{\rho h_p \omega_f^2}{D} = f(x,y) \quad (2)$$

where: $D = \frac{Eh^3}{12(1-\nu^2)}$ – flexural rigidity [Pa·m^4], w – transverse displacement of the plate [m], ω_f – excited frequency [rad/s], ρ – mass density [kg/m^3], h_p – plate thickness [m], E – Young's modulus [Pa], ν – Poisson's ratio, f – external forces [N], ∇ – biharmonic differential operator.

For the triangular plate under study, simply supported boundary conditions were assumed as a boundary condition on all three edges [19], Figure 1,

$$\begin{array}{lll} w(x,y) = M_x(x,y) = 0 & \text{for} & x = 0 \\ w(x,y) = M_y(x,y) = 0 & \text{for} & y = 0 \\ w(x,y) = M_h(x,y) = 0 & \text{for} & y = a - x \end{array} \tag{3}$$

where: $M_x = -D\left(\frac{\partial^2 w}{\partial x^2} + \nu \frac{\partial^2 w}{\partial y^2}\right)$ – bending moment along x axis, $M_x = -D\left(\frac{\partial^2 w}{\partial y^2} + \nu \frac{\partial^2 w}{\partial x^2}\right)$ – bending moment along y axis, $M_x = -D\left(\frac{\partial^2 w}{\partial h^2} + \nu \frac{\partial^2 w}{\partial n^2}\right)$ – bending moment along the hypotenuse of the right triangular plate, h – axis lying on the hypotenuse of the triangle, n – axis perpendicular to the hypotenuse, a – side length of the triangle.

External forcing was in the following distribution form,

$$f(x,y) = f_0 \delta(x - x_0, y - y_0) \tag{4}$$

where: f_0 – amplitude of the force, (x_0, y_0) – coordinates of the point force application.

The free vibration problem was solved using the superposition method for triangular plates, presented in [20, 21]. Applying this method to the problem involves forcing a given boundary condition on a given edge (e.g. regarding transversal displacement), then through the next building block another boundary condition is forced (e.g. regarding bending moment). The solution used two blocks, one forcing zero transversal displacement and the other forcing zero bending moment on a given axis. A simply supported boundary condition was forced e.g. on the $x = 0$ axis by overlapping these two blocks. This procedure was also applied to the $y = 0$ axis and by rotating the blocks by an angle of 45 degrees, to force a simply support on the hypotenuse of the right triangular plate. The calculated eigenvalues were in line with [21].

OPTIMISATION PROCEDURE

Before discussing the experiment, it should be noted that the shape of the optimal PZT was determined by mathematical modelling. In general, the optimisation was aimed at reducing vibration, so the main objective function was trivial and can be defined by:

$$J = \frac{w_0 - w_f}{w_0} \cdot 100\% \tag{5}$$

where: w_0 – transverse displacement of the plate without PZT action, vibration is excited by dis- turbance, [m]; w_f – transverse displacement of the plate with PZT action, vibration is excited by disturbance and reduced by PZT, [m].

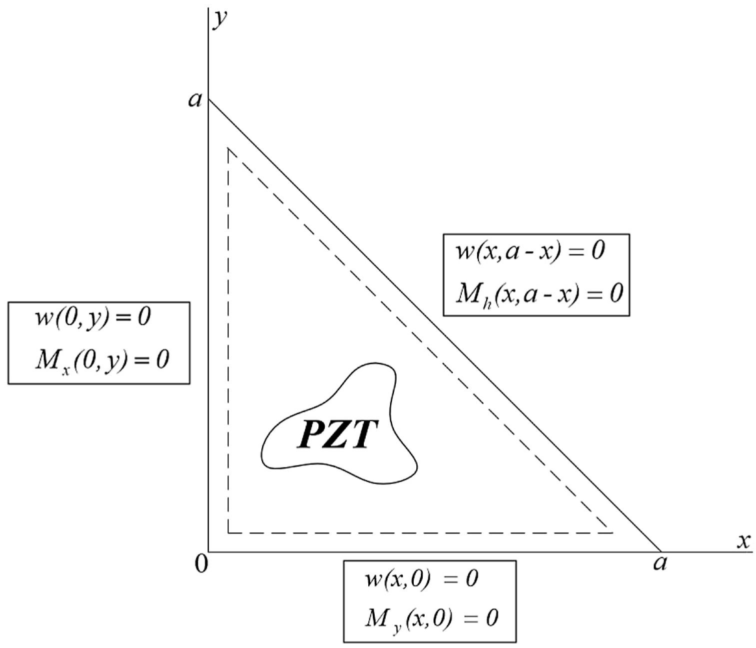

Figure 1. A simply supported right triangular plate

Mathematical modelling of PZT-plate interaction and introduction the new PZT model make it possible to formulate special forms of the objective function, which are given in [17]. The new model includes the possibility of adjusting the arm lengths of force pairs (which is not included in the classical PZT model [22, 23]). The results of the optimisation procedure for the first mode shape are shown in Figure 2. The location of all three actuators and the shape of the optimal PZT were determined. See [17] for figures of higher mode shapes.

EXPERIMENTAL SETUP

To experimentally verify the effectiveness of various PZT shapes, three actuators were ordered: s- PZT, c-PZT and a-PZT, Figure 3. Figure 4 shows the location of actuators on the plate surface and shapes of the compared PZTs for the first mode shape. To permanently fix the piezoelectric to the structure, a two-component adhesive was used.

Three identical triangular plates, each 1 mm thick, side length 0.2a and chamfered at 30 degrees along each edge, were fabricated. A different shaped PZT (square, circular, and asymmetrical) was glued to separate plate. The simply supported boundary condition was achieved on the basis of [9]. V-shaped groove with an angle of 90 degrees was milled into the designed plate mounting. The plate was chamfered at the edges at an angle of 30 degrees so that the edge of the plate lay in the milled groove, Figure 5. The joint between the plate and the frame had to be sealed, a universal silicone sealant was suggested in [10]. In the present work, the joint between the plate and the frame was sealed by means of heat-shrinkable

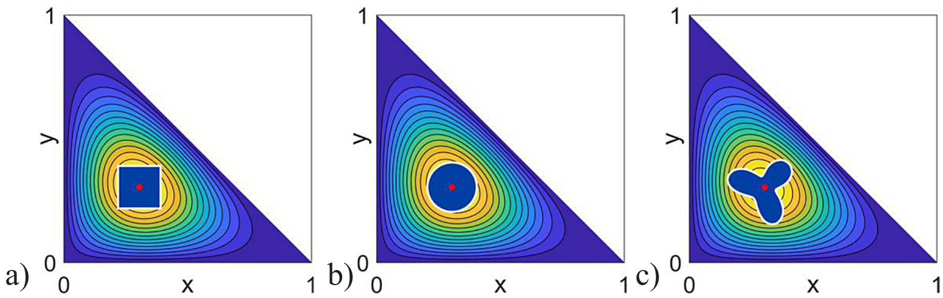

Figure 2. Location of symmetric actuators on surface of the triangular plate ((a) s-PZT, (b) c-PZT), location and shape of the a-PZT (c) [16]

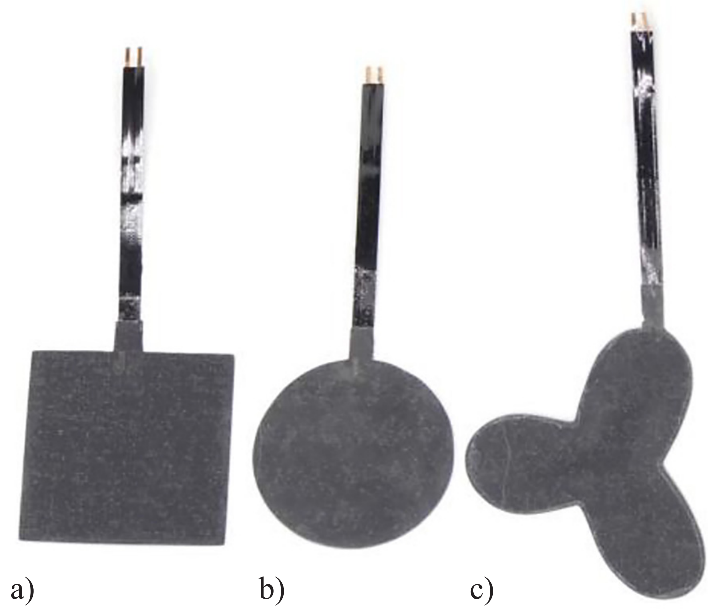

Figure 3. Shapes of actuators: s-PZT (a), c-PZT (b), a-PZT (c)

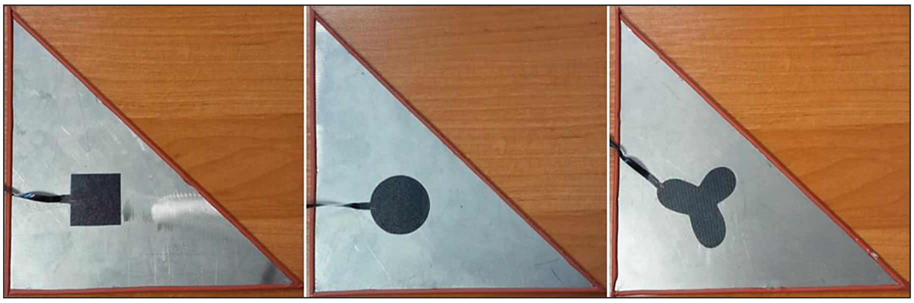

Figure 4. Placement of piezoelectric actuators on the surface of a triangular plate

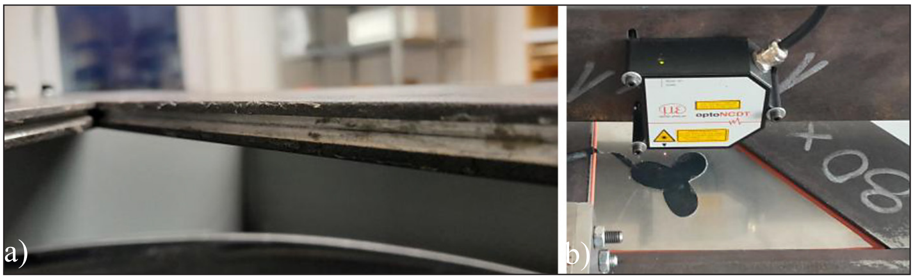

Figure 5. V-groove milled in the plate mounting (a), plate in the mounting (b)

sleeves placed on the edges of the plate. The first form of natural vibration of the plate was taken into account in the experiment.

The laboratory setup comprised a laptop computer, a 900 W Beyma 18G550 loudspeaker, an optoNCDT laser sensor, an MCP3008 external A/D converter, an ESP32 Dev Kit V1 development board, Korad KD3305P symmetrical power supply, a circuit consisting of operational amplifiers, EPA-104 power amplifier, PZTs and triangular plates. The vibration signal was measured over a range of 2 mm with a readout frequency of up to 20 kS/S. The NI USB-6212 Multifunctional I/O Device with BNC connectors was used to read the data, Figure 6.

The plates were mounted in steel frame screwed to a structure, inside which the loudspeaker was located. Beyma loudspeaker was mounted halfway up the steel structure, approximately 50 cm below the plate. An acoustic signal of given frequency was generated by loudspeaker to excite the plate to vibrate. This signal was sinusoidal signal fed to loudspeaker input via analog output channel of NI USB-6212. The amplitude of the plate vibrations was measured using optoNCDT optoelectronic sensor. The signal measured by

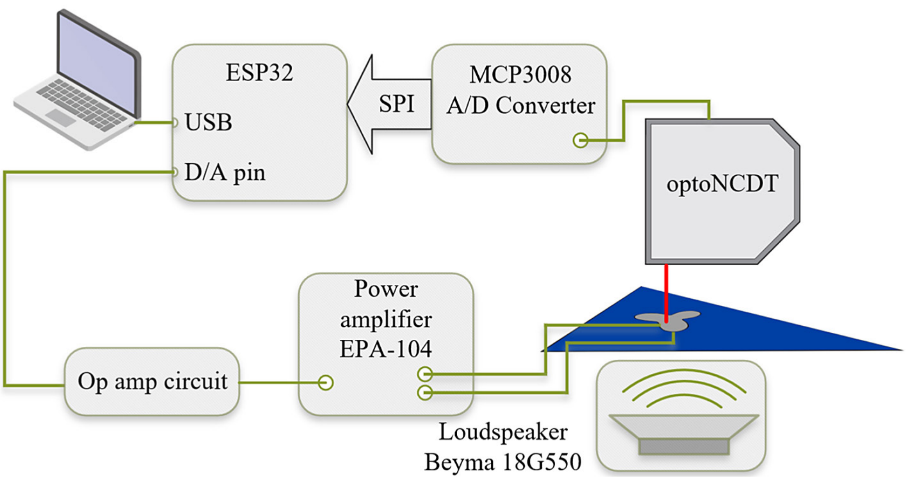

Figure 6. Laboratory setup

sensor was the input to active vibration reduction algorithm implemented on ESP32-DevKit V1 development board. However, before the analog signal from the sensor was processed by AVC algorithm, it is read by external ADC (MCP 3008) connected to ESP32 via SPI interface. This transducer reads the signal in differential mode [24]. In next step, the signal was processed by AVC algorithm and directed from the ESP32 board to amplifier circuit via an internal digital-to-analog converter. The circuit composed of operational amplifiers provides the first level of amplification for the output signal. The diagram of the designed circuit is illustrated in Figure 7.

The second important function of this circuit, apart from amplification, was to provide negative offset for output signal. Since the ESP32 board does not allow generating bipolar signal for built-in DAC, it was necessary to generate an unipolar signal and add negative DC component. The circuit was built using NE5532 operational amplifiers [25] and designed in PSIM software [26]. In order to create negative DC component, it was necessary to supply the amplifier circuit with symmetrical power supply. The Korad KD3305P power supply was used for this purpose. An EPA-104 power amplifier, designed as PZT amplifier, was placed after amplifier circuit. The prepared and amplified signal was used to power the PZT. Data acquisition was performed using NI USB-6212 connected to computer with MATLAB software.

The experiment involved implementing a feedback system with a PI controller. The system responded to a disturbance in the form of an acoustic wave, which was generated by a loudspeaker, Figure 8. The controller was implemented using C language on ESP32 development board. The program calculated the output to the PZT actuator based on the reading and the applied PI tuning parameters [27].

RESULTS

Analytical and numerical calculations were conducted to determine the most efficient shape under steady-state conditions [17]. It turned out that the most effective PZT was a-PZT and its advantage over regular shapes was up to several percent, depending on the mode shape. For example, the results obtained in [17] for first mode

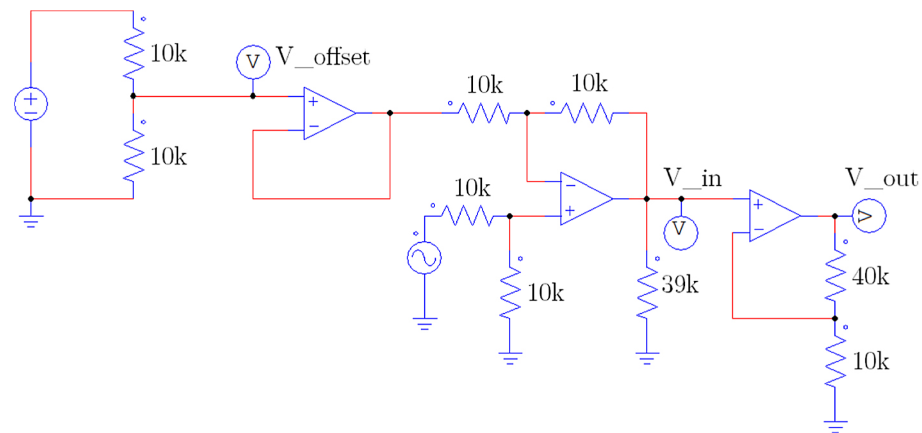

Figure 7. Signal amplification circuit designed in PSIM software

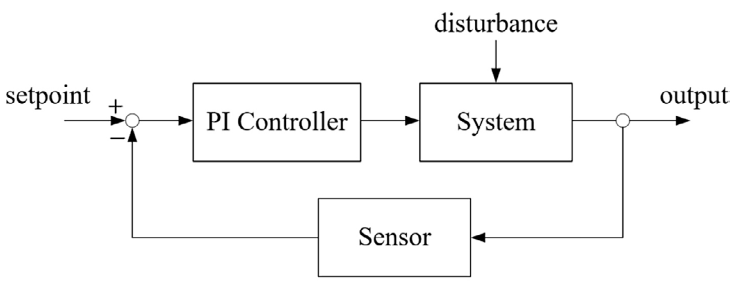

Figure 8. Feedback control system used in the experiment

shape were: for s-PZT – 97.43%, for c-PZT – 97.70%, and for a-PZT – 99.96%.

In the cited work, a relative vibration reduction coefficient was used, hence it was expressed as a percentage. To confirm these results, an active vibration control algorithm was implemented and experimentally verified.

This paper also verified the implementation of the simply supported boundary condition for triangular plate. To achieve this, the values of the natural frequencies of the plate were compared. The eigenvalue λ^2 expressed in the Gorman superposition method does not depend on the thickness of the plate. To verify the values obtained for a plate of given dimensions, the thickness of the plate should be taken into account in the eigenvalue expression: $\lambda^2 = \omega a^2 \sqrt{\rho h_p / D}$. Using this expression, one can calculate the eigenfrequencies ω, Table 1. The Gorman method does not take into account the modification of the geometry of the triangular plate in the form of a 30 degree chamfer. For this purpose, a 3D model of the plate was created taking into account a 30 degree chamfer on all edges and calculations were performed in ANSYS environment for simply supported boundary conditions on all edges of the plate, Table 1. 7201 second order tetrahedral elements were used in the FEM analysis, for a total of 44455 degrees of freedom.

Experimental results

The scope of the experiment was to determine the frequency response of the plates: with the disturbance from the loudspeaker and with the active vibration reduction system switched on. The active vibration reduction system included three types of PZT: s-PZT, c-PZT and a-PZT. Each actuator operated at a constant hardware gain, while the software gain was adjusted to keep the system stable. Hardware gain was the gain included in circuit consisting of operational amplifiers and the maximum gain provided by the EPA-104 power amplifier. The first test was to see if three identical plates gave the same frequency response to loudspeaker excitation. Figure 9 shows the results. Although all the plates have the same dimensions and are manufactured in the same way, there are slight differences in the characteristics obtained [28]. The first eigenfrequency of the plate with s-PZT was 279 Hz, for a-PZT it is 280 Hz and for c-PZT it was 281 Hz. By averaging the results obtained, the value of 280 Hz was taken as the first natural frequency of the plate, see Table 2.

The next step was to investigate the effectiveness of active vibration reduction at constant hard- ware and software gain for the tested actuators. For this purpose, the gain of the proportional term of the PI controller was set to 1.2 (this value was chosen experimentally). The gain of the integrating term was set to 0.01 for all actuators. The hardware gain of the EPA-104 amplifier was the same for all experiments performed and was 20. Figure 10 shows the frequency response results of a feedback system with a PI controller for s-PZT.

Figures 11–12 show the frequency response of the closed loop control signal for c-PZT and a- PZT respectively. All three figures show effective vibration reduction and a significant reduction in amplitude at the resonant frequency. However, comparing the three frequency responses confirms that a-PZT was characterised

Table 1. Natural frequencies for the first six mode shapes calculated by Gorman method and using the ANSYS environment

Parameter	Mode shape				
	1	2	3	4	5
$\omega_{v;Gorman}$ [Hz]	296.78	593.57	771.64	1009.07	1187.14
$\omega_{v;ANSYS}$ [Hz]	295.31	592.17	770.43	1010.40	1189.20

Table 2. Relative errors in the value of the first natural frequency of the triangular plate

Parameter	First natural frequency of the plate		
	Analytically	ANSYS	Experiment
ω_v [Hz]	296.78	295.31	280.00
Relative error [%]	–	0.4953	5.6540

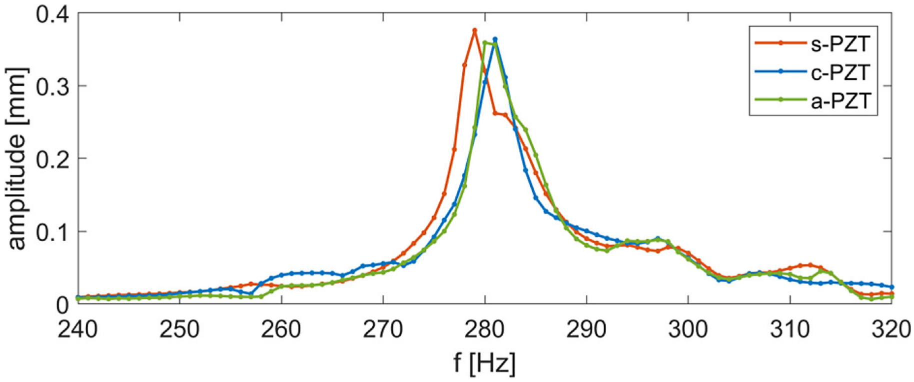

Figure 9. Frequency response to loudspeaker disturbance for three plates with three different PZTs: s-PZT, c-PZT and a-PZT

by the highest efficiency over almost the entire range tested, Figure 13.

The time courses for resonant frequency is presented in Figures 14–16. The time at which active vibration reduction system was switched on was set to t_{ON} = 5 s.

The last point of experiment was to adjust the software gain level to the stability limit. For this purpose, the gain values of the proportional part of the PI controller were experimentally set to obtain a critical gain. This experiment was carried out to justify that any type of actuator is capable of reducing vibrations to a relatively low level. The difference is that a higher signal gain is required and therefore the control signal has a higher energy, so a higher energy supply must also be provided to achieve a given level of reduction, Figure 17. Thus, for s-PZT the gain level was $K_{P;s-PZT}^{cr}$ = 1.80, for c-PZT $K_{P;c-PZT}^{cr}$ = 3.20 and for a-PZT – $K_{P;a-PZT}^{cr}$ = 1.22.

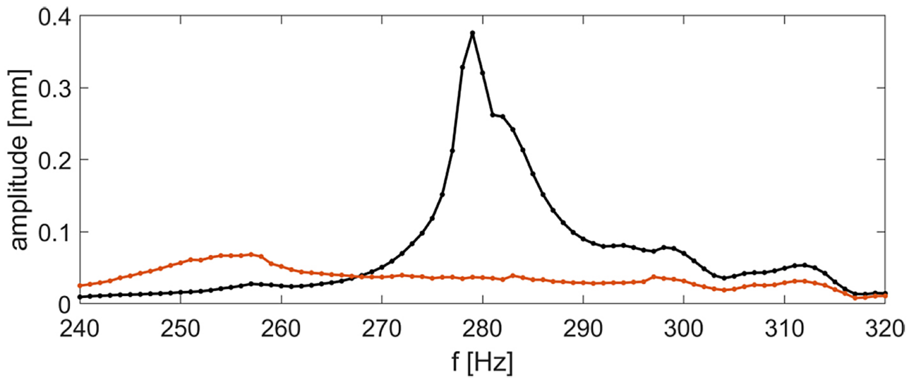

Figure 10. Frequency response of open-loop (black) and closed-loop (red) signals for s-PZT with K_P = 1.2

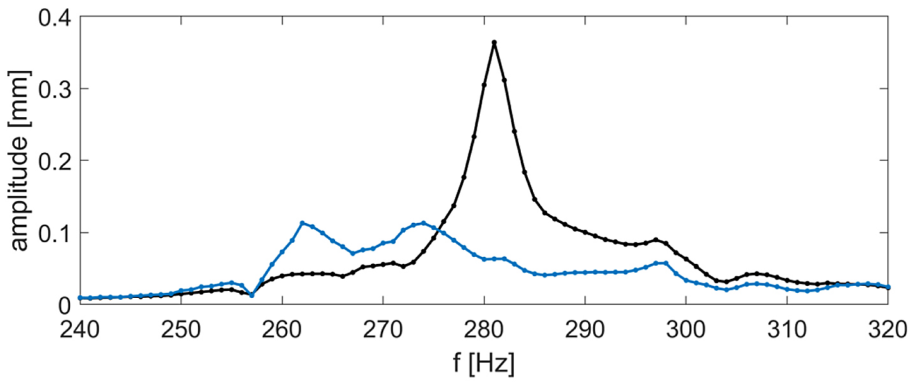

Figure 11. Frequency response of open-loop (black) and closed-loop (blue) signals for c-PZT with K_p = 1.2

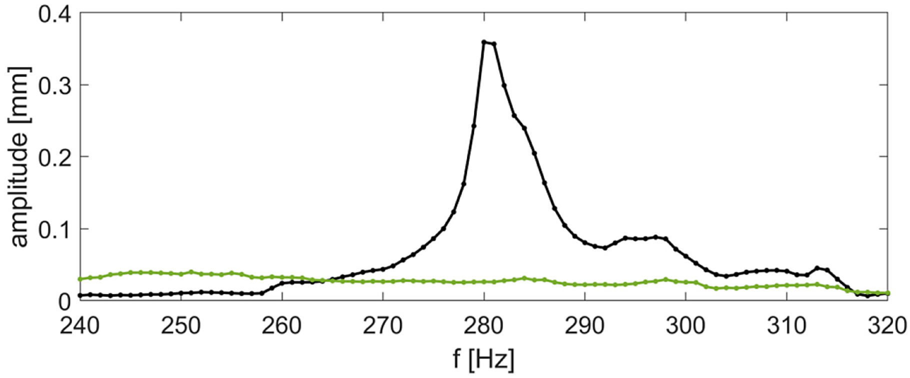

Figure 12. Frequency response of open-loop (black) and closed-loop (green) signals for a-PZT with $K_p = 1.2$

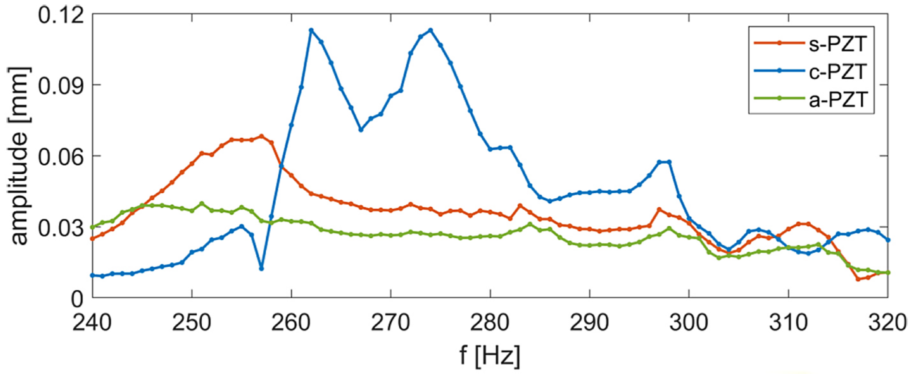

Figure 13. Closed-loop frequency responses for three actuators with gain $K_p = 1.2$: s-PZT, c-PZT and a-PZT

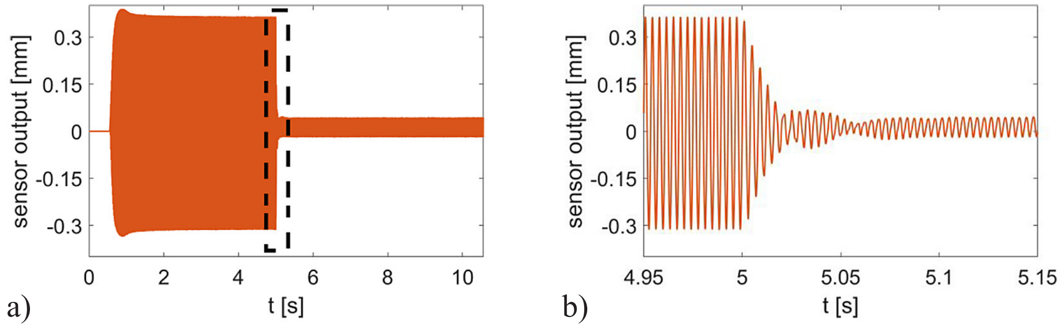

Figure 14. Time course of s-PZT with K_p = 1.2 (a). Close-up of part of the graph (marked with black dashed frame) showing the moment of AVC activation (b)

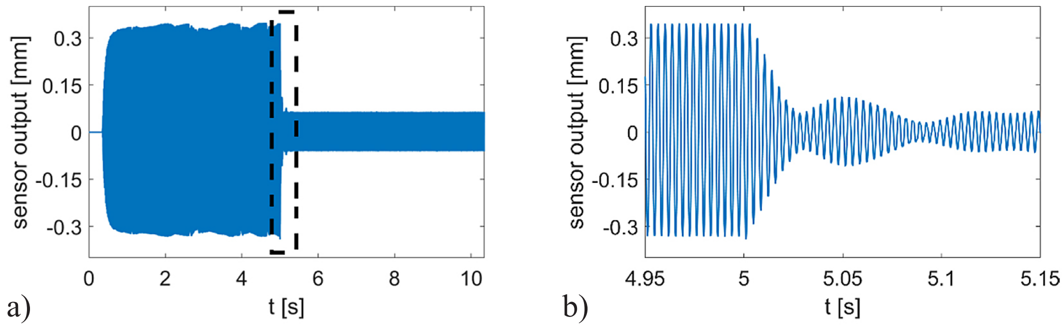

Figure 15. Time course of c-PZT with K_p = 1.2 (a). Close-up of part of the graph (marked with black dashed frame) showing the moment of AVC activation (b)

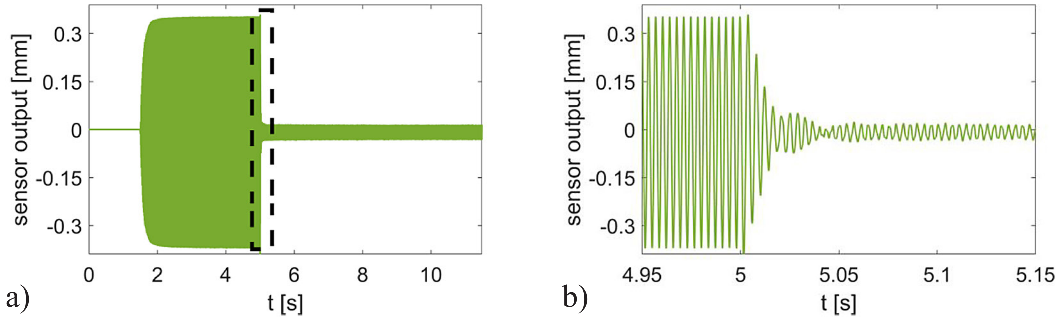

Figure 16. Time course of a-PZT with $K_P = 1.2$ (a). Close-up of part of the graph (marked with black dashed frame) showing the moment of AVC activation (b)

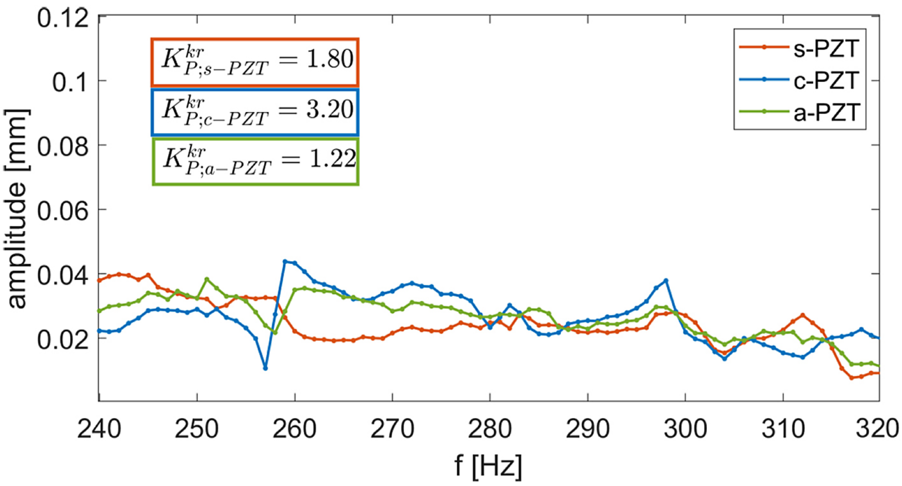

Figure 17. Closed-loop frequency responses for three actuators with critical gain level

CONCLUSIONS

The article examined the use of different shapes of piezoelectric actuators in active vibration control of triangular plates. The study compared three types of actuators: circular and square, which are commonly used shapes, and an asymmetric actuator, which provided the highest vibration reduction efficiency. The shape of the a-PZT was determined through analytical and numerical calculations [17].

On the basis of the analytical, numerical and experimental studies conducted, following conclusions can be made. First, the most important conclusion is that for the same energy applied to the system with different types of PZT, the system with a-PZT was the most effective in reducing the vibrations of the triangular plate. The amplitude of the vibrations generated by the excitation of the acoustic wave from the loudspeaker was approximately 0.35 mm and was reduced to approximately 0.02 mm. By adjusting the proportional gain level within the stability criterion, even better results can be achieved. It is worth noting that the experimental results are consistent with the analytical and numerical results, i.e. the plate with a-PZT was characterised by the highest efficiency both in the steady state and taking into account the dynamics of active vibration reduction.

Second, the plate with s-PZT installed had better results than the plate with c-PZT in almost the whole range tested. The results presented in Figure 13 show that at the beginning of tested range, i.e. from 240 Hz to 260 Hz, better results are obtained by using c-PZT. However, first natural frequency of the plate and frequencies close to it are the more important part of frequencies tested. In this range there is a clear drop in c-PZT efficiency, which includes frequencies from 260 Hz to 308 Hz, followed by a short period of slight advantage for the c-PZT and again a drop in efficiency in favour of s-PZT. For first natural frequency, $f = 280$ Hz, we have c-PZT efficiency of 79.42%, with s-PZT efficiency of 88.71% and an a-PZT efficiency of 92.74%. Thus, the experimental results do not coincide with the numerical results for this range. This may be due to imperfections in the manufacture of the plate or in the bonding of the actuators, or in the realisation of simply supported boundary condition for the plate with c-PZT. However, c-PZT was less effective than a-PZT, which confirms the first conclusion.

Another conclusion relates to the critical damping experiments. The research confirms that a-PZT requires less amplification of input signal to achieve relatively similar level of vibration reduction. It is therefore the most efficient in terms of energy consumption.

This paper presents a feasible approach for designing piezoelectric actuators to reduce vibrations in plates of various shapes. The study on this topic is still developing and many other issues deserve further investigation. For example, finding the optimal shape of a piezoelectric actuator for solid structures or other three-dimensional ones such as trusses, shells.

Acknowledgement

This research did not receive any specific grant from funding agencies in the public, commercial, or not-for-profit sectors.

REFERENCES

1. Wang W. Electrode shape optimization of piezoelectric transducers, Ph.D. Thesis, University of Florida; 2003.
2. Zhang X., Takezawa A., Kang Z. Topology optimization of piezoelectric smart structures for minimum energy consumption under active control. Struct. Multidiscip. O. 2018; 58: 185–199. https://doi.org/10.1007/s00158-017-1886-y
3. Donoso A., Sigmund O. Optimization of piezoelectric bimorph actuators with active damping for static and dynamic loads. Struct. Multidiscip. O. 2009; 38: 171–183. https://doi.org/10.1007/s00158-008-0273-0
4. Gonçalves J.F., De Leon D.M., Perondi E.A. Topology optimization of embedded piezo- electric actuators considering control spillover effects. J. Sound Vib. 2017; 388: 20–41. https://doi.org/10.1016/j.jsv.2016.11.001
5. Aridogan A., Basdogan I. A review of active vibration and noise suppression of plate-like structures with piezoelectric transducers. J. Intel. Mat. Syst. Str. 2015; 26(12): 1455–1476. https://doi.org/10.1177/1045389X15585896
6. Al-Obiedy A.N., Al-Helli A.H. A review of the state-of-the-art in improving piezoelectric properties. Adv. Sci. Tech. Res. J. 2025; 19(6): 41–69. https://doi.org/10.12913/22998624/202784
7. Liu Y., Xiao D. Shape feature controller topology optimization of attached piezoelectric ac- tuators for vibration control of thin-walled smart structures. Appl. Math. Model. 2023; 89(1): 107–118. https://doi.org/10.1016/j.apm.2023.03.018
8. Pavelka V., Suranek P., Strambersky R. Thin Plate Active Vibration Control. In: 22nd In- ternational Carpathian Control Conference (ICCC). Velké Karlovice, Czech Republic; 2021. https://doi.org/10.1109/ICCC51557.2021.9454648
9. Trojanowski R., Wiciak J. Impact of the size of the sensor part on sensor-actuator efficiency. J. Theor. App. Mech.-Pol. 2020; 58(2): 391–401. https://doi.org/10.15632/jtam-pl/118948
10. Dumond P., Monette D., Alladkani F., Akl J., Chikhaoui I. Simplified setup for the vibration study of plates with simply-supported boundary conditions. MethodsX 2019; 6: 2106–2117. https://doi.org/10.1016/j.mex.2019.09.023
11. Koszewnik A. The active vibration control of the plate structure by using LQG controller and piezo-stripes. In: 22nd International Conference on Methods and Models in Automation and Robotics (MMAR), Miedzyzdroje, Poland; 2017. https://doi.org/10.1109/MMAR.2017.8046930
12. Muthalif A.G.A., Nor K.A.M., Wahid A.N., Ali A. Optimization of Piezoelec- tric Sensor-Actuator for Plate Vibration Control Using Evolutionary Computation: Modeling, Simulation and Experimentation. IEEE Access 2021; 9: 100725–100734. https://doi.org/10.1109/ACCESS.2021.3096972
13. Rahman T.A.Z., Darus I.Z.M. Experimental evaluation of Active Vibration Control of a flexible plate using proportional gain controller. In: IEEE Symposium on Industrial Electronics and Applications, Langkawi, Malaysia; 2011. https://doi.org/10.1109/ISIEA.2011.6108736
14. Wrona S., Pawełczyk M. Controllability-Oriented Placement of Actuators for Active Noise- Vibration Control of Rectangular Plates Using a Memetic Algorithm. Arch. Acoust. 2013; 38(4): 529–536. https://doi.org/10.2478/aoa-2013-0062
15. Brański A., Kuras R. Asymmetrical PZT applied to active reduction of asymmetri- cally vibrating beam – semi-analytical solution. Arch. Acoust. 2022; 47(4): 555–564. https://doi.org/10.24425/aoa.2022.142891
16. Kuras R. Influence of the PZT actuator asymmetry on the lqr control parameters in the active reduction vibrations of beams. Vib. Phys. Syst. 2022; 33(3): 2022305. https://doi.org/10.21008/j.0860-6897.2022.3.05
17. Brański A., Kuras R. PZT asymmetrical shape optimization in active vi- bration reduction

of triangular plates. Arch. Acoust. 2023; 48(3): 425–432. https://doi.org/10.24425/aoa.2023.145241

18. Rao S.S. Vibration of Continuous Systems. John Wiley & Sons Inc., Hoboken, New Jersey; 2007.
19. Leissa A.W. Vibration of plates. Scientific and Technical Information Division NASA, Wash- ington; 1969.
20. Gorman D.J. Vibration analysis of plates by the superposition method. World Scientific Publishing Co. Pte. Ltd., Singapore; 1999.
21. Saliba H.T. Transverse free vibration of simply supported right triangular thin plates: a highly accurate simplified solution. J. Sound Vib. 1990; 139(2): 289–297. https://doi.org/10.1016/0022- 460X(90)90889-8
22. Fuller C.R., Elliot S.J., Nielsen P.A. Active control of vibration. Academic Press, London; 1997.
23. Hansen C.H., Snyder S.D. Active control of noise and vibration. E & FN SPON, London; 1997.
24. Nelson C. MCP3008 8-Channel 10-Bit ADC, GitHub, 2021. https://github.com/ adafruit/Adafruit_MCP3008 (accessed 20 March 2025).
25. Texas Instruments Inc., NE5532x, SA5532x Dual Low-Noise Operational Amplifiers, 2015. https://www.ti.com/lit/gpn/NE5532A (accessed 20 March 2025).
26. Powersim Inc. PSIM User's Manual, 2020. https://www.powersimtech.com.
27. Matera M. FastPID, GitHub, 2019. https://github.com/mike-matera/FastPID (accessed 20 March 2025).
28. Kuras R., Hajder S. Experimental validation of the asymmetric PZT optimal shape in the ac- tive vibration reduction of triangular plates. Int. J. Electron. Telecomm. 2024; 70(3): 563–568. https://doi.org/10.24425/ijet.2024.149579